RESEARCH ACTIVITIES III
Department of Electronic Structure

III-A States of Molecular Associates in Aqueous Environment

Because of its large dipole moment, smallness of the molecule, and structure making and network formation abilities, water can dissolve various molecules in the liquid state. Although we know phase separation of hydrophobic liquids from aqueous solutions at critical concentrations, it is not so well understood how solute molecules are dissolved in water, particularly at a solute molar fraction in the region of 10^{-2}-10^{-3}. Despite of extreme importance of the study on the intermolecular interaction in the solution, spectroscopic approach for capturing evident structural information has been limited to provide indirect information on the states of molecular associates. In particular, the observation of intermolecular vibrations in solution systems is highly important, although the depolarized Rayleigh wing spectra are normally just broad and give almost structureless feature. The development of theoretical approach and the use of $R(\bar{\nu})$ representation for the Raman spectra has changed this situation drastically. For the development of a new type of spectroscopy by means of synchronized femto (low resolution) and pico(high resolution) multi-beam laser system, our study is now concentrated to finding good molecular systems with interesting and functional molecular association in the aqueous environment.

III-A-1 Low Frequency Raman Spectra of Crystalline and Liquid Acetic Acid and its Mixtures with Water: Is the Liquid Dominated by Hydrogen-Bonded Cyclic Dimers?

Kentaroh KOSUGI *(Grad. Univ. Adv. Stud.)*, **Takakazu NAKABAYASHI and Nobuyuki NISHI**

[*Chem. Phys. Lett.* **291**, 253 (1998)]

Crystalline acetic acid has a melting point at 16.6 ˚C (= 289.8 K). The crystalline structure has a chain form with the C=O oxygen atom doubly coordinated with an O-H hydrogen atom of a neighboring acetic acid and a methyl hydrogen of another molecule. Low frequency Raman spectra of crystalline and liquid acetic acid are presented in the form of the relative scattering activities, $R(\bar{\nu})$ spectra in Figure 1. The crystalline spectrum at 286 K shows five distinctive bands at 48, 78, 91, 122, and 180 cm^{-1}, and at least two weak bands at 30, and 40 cm^{-1}. The 78 and 91 cm^{-1} bands show difference in the polarization. At a specific crystal angle these bands become as strong as other three bands. Upon the melting of the crystal, however, the liquid exhibits conspicuous difference in its appearance. The intensity at lower frequencies increases drastically and a new but weak component appeared at 170 cm^{-1}. However, the main spectral feature is unchanged on the melting: the $R(\bar{\nu})$ spectrum of the liquid shows two strong peaks and a shoulder at wavelengths similar to those of the crystalline bands. The spectral change does not directly support the dominance of the cyclic dimers in the liquid. We attribute the observed and analyzed components to the fragment clusters with structures similar to the parts of the crystalline networks.

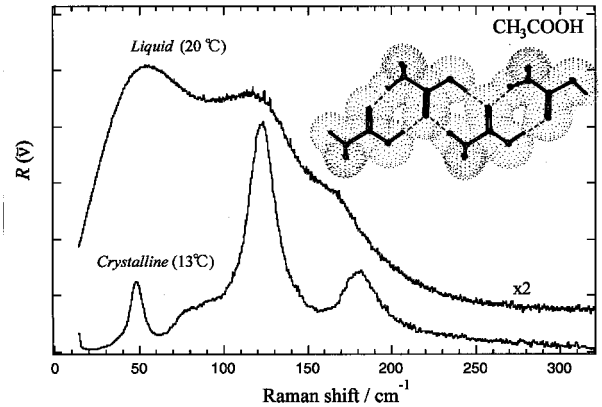

Figure 1. $R(\bar{\nu})$ spectra of crystalline acetic acid at 13 ˚C (bottom) and liquid acetic acid at 20 ˚C (top).

III-A-2 Effects of Intermolecular Hydrogen-Bonding Interactions on Raman Spectra of Crystalline and Liquid Acetic Acid: Ab Initio Molecular Orbital Study

Takakazu NAKABAYASHI, Kentaroh KOSUGI *(Grad. Univ. Adv. Stud.)* **and Nobuyuki NISHI**

Hydrogen bonding molecular crystals usually melt with a heat of fusion fairly smaller than the energy of hydrogen bonding. An ice melts with 25% of a single hydrogen bond energy, while acetic acid melts with 20% of the dimerization energy. This indicates that the liquid maintains large parts of the network structure as clusters, fragments of the chains. We observed the change of the low-wavenumber Raman spectrum of acetic acid on melting and came to assign the peaks to the clusters with structures similar to that of the crystal. In order to confirm this assignment we performed ab initio molecular orbital calculations of intermolecular vibrational wavenumbers and their Raman intensities of various clusters of acetic acid. The calculated low-wavenumber Raman spectra ($R(\bar{\nu})$ representation) for the cluster species at the HF/6-31G(d,p) level are shown

in Figure 1. The observed $R(\bar{\nu})$ spectrum of solid acetic acid is also shown in this figure. Crystalline acetic acid has been shown to have infinite chains, which involve C-H···O as well as O-H···O hydrogen bonds. The intensity pattern in the $R(\bar{\nu})$ spectrum of solid acetic acid is well reproduced by the $R(\bar{\nu})$ spectra calculated for the chain clusters which contain C-H···O and O-H···O hydrogen bonds. The features of the $R(\bar{\nu})$ spectra calculated for the chain clusters are independent of the aggregate size, but are different from the spectrum of the cyclic dimer which contains two O-H···O hydrogen bonds. The melting of the solid leads to a broadening of the $R(\bar{\nu})$ spectrum and an increase in the intensity in the low-wavenumber region (≈ 50 cm^{-1}), however, it does not affect the main peak positions of the $R(\bar{\nu})$ spectrum. These spectral changes are reproduced by the $R(\bar{\nu})$ spectra calculated on the assumption that a variety of chain sizes are produced on the melting of the solid. From the results described above, we conclude that the liquid acetic acid is mainly composed of the chain clusters, not the cyclic dimer, near the temperature of the melting point and at room temperature. On going from the solid to the liquid state, the C=O stretching band (≈ 1670 cm^{-1}) becomes broadened toward the higher-wavenumber side and exhibits an obviously asymmetric shape. This result is attributable to the increase in the number of C=O bonds which are shortened due to weakened hydrogen bonding interactions with the breaking of the chain on the melting. Calculated frequencies of the C=O stretches for the clusters support the above conclusion.

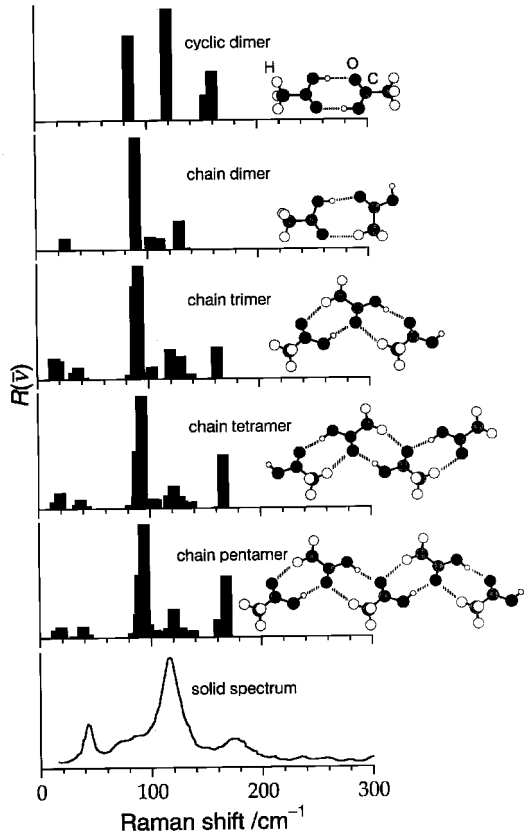

Figure 1. Optimized geometries and $R(\bar{\nu})$ spectra of the cluster species of acetic acid. Observed $R(\bar{\nu})$spectrum of solid acetic acid is shown in the bottom.

III-A-3 States of Acetic Acid and Water Molecules in Aqueous Mixture Studied by Low Frequency Raman Spectroscopy

Kentaroh KOSUGI *(Grad. Univ. Adv. Stud.)*, **Takakazu NAKABAYASHI and Nobuyuki NISHI**

Acetic acid has been believed to form a cyclic dimer with the methyl groups at the both ends even in aqueous solution. From the theoretical point of view, such a cyclic dimer with a negligible dipole moment is hardly stabilized in polar environment. Figure 1 shows the spectral change in $R(\bar{\nu})$ representation of acetic acid-water binary mixtures with varying molar fraction of acetic acid (χ_A). The $R(\bar{\nu})$ spectra at $0 < \chi_A < 0.5$ are found to be reproduced by linear combinations of the spectra at $\chi_A = 0$ and 0.5, indicating that the intermolecular compounds responsible for the Raman signals contain the same structure (or intermolecular bindings) in this concentration range. Interestingly, the $R(\bar{\nu})$ spectrum of acetic acid-methanol mixture with $\chi_A = 0.5$ shows nearly the same spectral shape except for the some intensity extension on the lower energy side and methanol signals around 250 cm^{-1}. This spectral similarity in the two systems strongly suggests that an acetic acid dimer pair or a dimer structure is responsible for the spectra. Intermolecular vibrational frequencies and Raman intensities are calculated by Gaussian 94 at the HF/6-31G(d,p) level. The structure that reproduces the observed Raman spectrum is inserted in Figure 1. The two acetic acids are not equivalent to each other. One C=O is hydrogen-bonded, while the other C=O is free producing a large dipole moment as a dimer. This result is in accord with the spectral change of the intramolecular C=O stretching band on varying the acid concentration. The asymmetric band around 1700 cm^{-1} observed for the mixture with $\chi_A = 0.3$ is decomposed into two components: a narrow band at 1715 cm^{-1} and a broad band with a peak at 1685 cm^{-1} and an extended wing to the lower frequencies. The former component is attributed to non-bonded C=O and the latter to the hydrogen-bonded C=O. Most interestingly, the O-H stretching bands of water exhibit that hydrogen bonds of waters are dissociated with increasing the acid.

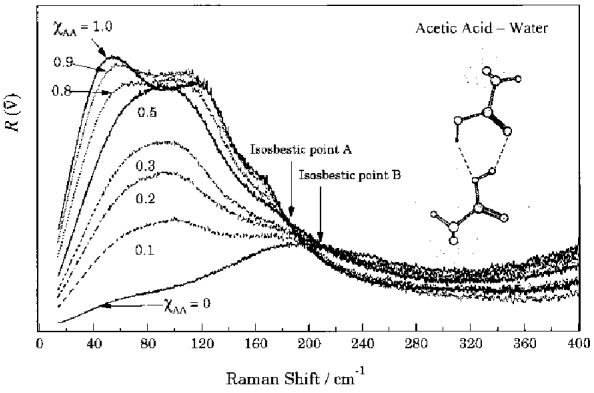

Figure 1. Mixing ratio dependence of the $R(\bar{\nu})$ spectra in acetic acid -water binary system.

III-B Spectroscopic and Dynamical Studies on Charge Delocalization and Charge Transfer in Aromatic Molecular Clusters

Charge transfer processes resulting in dynamical charge delocalization such as consecutive proton or electron hopping in molecular clusters and even in pure liquids are highly interesting in relation to the charge transportation in insulating materials. Not only in aromatic molecular liquids but also in pure water itself electric conductivity is very low when they do not contain impurities of ionic atoms or molecules. We demonstrated that a positive charge in a pure benzene cluster is localized in a dimer unit where the charge resonance (CR) interaction makes the two molecules share an electron forming an intermolecular bond. One of the hot topics in this project is the finding of the charge hopping in vibrationally excited benzene trimer cations. This means the dimer cation core in the trimer is switching, probably periodically concerted with an asymmetric stretching motion of the three benzene molecules.

III-B-1 Vibrational Predissociation Spectroscopy of Phenol-Benzene Dimer Cation

Yoshiya INOKUCHI, Nobuyuki NISHI and James M. LISY *(Univ. Illinois and IMS)*

Vibrational predissociation spectroscopy is one of the most powerful methods to investigate geometric structures of cluster ions. In a hetero-dimer cation of (phenol-benzene)$^+$, the charge is expected to be localized on the phenol site. Then, the hydrogen atom of the hydroxyl group is thought to be coordinated with the π-electron cloud of the neutral benzene. In order to examine this situation, we have measured a vibrational predissociation spectrum of (phenol-benzene)$^+$ in the region of 2900-3500 cm^{-1}. The experiment is done by using a tandem mass spectrometer, which consists of two quadrupole mass analyzers. Mass-selected ions of (phenol-benzene)$^+$ are irradiated with an IR output of a commercial OPO laser. The photoexcited dimer cation immediately dissociates into a cation and a neutral. Resultant fragment phenol ions are mass-analyzed and detected by an MSP. Thus, the vibrational predissociation spectrum of the dimer cation is obtained from the yields of the fragment ions with varying the excitation laser wavenumber.

A photodissociation study of (phenol-benzene)$^+$ in the 750-1250 nm region already showed that the positive charge is localized on the phenol site. Such an electronic spectrum, however, cannot provide detailed information on the structure of cluster ions. Figure 1 shows a vibrational predissociation spectrum of (phenol-benzene)$^+$. The spectrum shows a single peak at 3239 cm^{-1} and the apparent width of 67 cm^{-1} (FWHM). The peak can be attributed to the OH stretching vibration of (phenol-benzene)$^+$. The reported OH stretching frequency of a bare phenol ion is 3534 cm^{-1}. The observed OH stretching frequency of the dimer cation shows a 295-cm^{-1} red-shift from that of the bare phenol ion. The red shift indicates that the hydrogen atom of the hydroxyl group is coordinated with the π-electrons of the benzene. Such a π-hydrogen bonding is known in benzene-water or benzene - methanol neutral clusters. The present result disagrees with the spectrum reported by Mikami and co-workers. In their spectrum, a peak emerges at 3060 cm^{-1} with a width of approximately 120 cm^{-1} (FWHM), almost twice as large as the present observation. The difference in the spectra is thought to be originated from the difference of the temperature of the cluster ions. Now we are investigating such a large temperature effect on the structure of the cations.

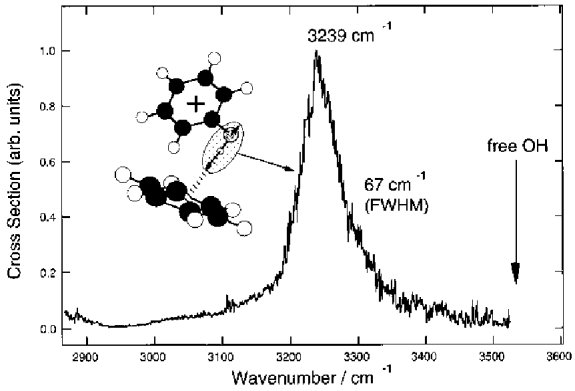

Figure 1. Vibrational predissociation spectrum of (benzene-phenol)$^+$.

III-B-2 Electronic Structure of Solvent Benzene in (Phenol-Benzene)$^+$

Yoshiya INOKUCHI, Nobuyuki NISHI and James M. LISY *(Univ. Illinois and IMS)*

Presence of a π-hydrogen bond in (phenol-benzene)$^+$ is expected to perturb the electronic structure of benzene chromophore. The electronic structure of solvent benzene in (phenol-benzene)$^+$ has been investigated by photodissociation spectroscopy in the region of 23500-40650 cm^{-1} where the electronic transitions of neutral benzene and cationic phenol are expected to appear.

First in order to find the absorption bands of phenol ion chromophore, the electronic spectrum of (phenol-water)$^+$ was observed by the photodissociation method. In this cluster, the charge is localized on phenol. Thus, we assumed that the observed electronic spectrum is characteristic of the phenol cation. The phenol cation spectrum is subtracted from the photodissociation spectrum of (phenol-benzene)$^+$. Figure 1 shows the subtracted spectrum, which is regarded as an electronic spectrum of benzene site in (phenol-benzene)$^+$. This absorption band is ascribed to the $\pi^* \leftarrow \pi$ transition of the benzene site. The $\pi^* \leftarrow \pi$ transition of the benzene site in (phenol-benzene)$^+$ is approximately 1600-cm^{-1} red-shifted from that of the neutral benzene. Such a

large red-shift of the $\pi^* \leftarrow \pi$ transition could be an evidence that the π-orbitals of the benzene are perturbed so much because of the π-hydrogen bonding. In Figure 1, an absorption spectrum of benzene vapor is also shown for comparison with the positional shift by 1600 cm^{-1} to the red from the original position. From the comparison of these spectra, one can find that the vibrational sequence in the cluster spectrum is almost the same as that of benzene vapor spectrum, except for the band at 36470 cm^{-1}. On the basis of the spacing corresponding to the ν_6 and ν_1 vibrations, this band is attributed to the 0-0 band of the $\pi^* \leftarrow \pi$ transition. In a benzene-water neutral dimer with a π-hydrogen bond, the 0-0 band is not observed because the sixfold symmetry of benzene is kept due to the free rotation of the water molecule along the sixfold axis. In (phenol-benzene)$^+$, therefore, the interaction between the positive charge on the aromatic ring of phenol ion and the π-electrons of neutral benzene may fix the intermolecular configuration, strongly breaking the sixfold symmetry.

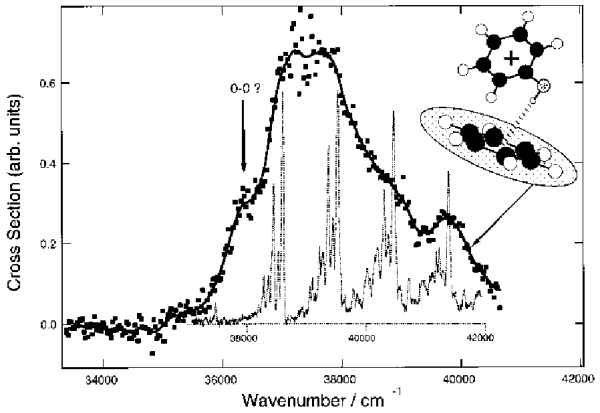

Figure 1. Electronic spectrum of the benzene chromophore in (phenol-benzene)$^+$ and absorption spectrum of benzene vapor (dotted curve).

III-B-3 Photodissociation Dynamics of $(C_6H_6)_3^+$: Role of the Extra Benzene Molecule Weakly Bound to the Dimer Core

Kazuhiko OHASHI *(Kyushu Univ. and IMS)* **and Nobuyuki NISHI**

[*J. Chem. Phys.* in press]

Benzene trimer ion has a charge-localized structure, $(C_6H_6)_2^+\cdots C_6H_6$, where $(C_6H_6)_2^+$ is the dimer core. The trimer ion is photodissociated by excitation of the charge resonance transition of the dimer core. Branching ratios and translational energies of the product ions, $(C_6H_6)_2^+$ and $C_6H_6^+$, are measured as functions of photon energies ($h\nu$ = 0.99-1.80 eV). At the lowest photon energy studied, the dominant dissociation channel is the formation of $(C_6H_6)_2^+$ and C_6H_6. In this process, only a small fraction (7-8 %) of the available energy is partitioned into the translational energy of the products. The branching ratio of the $(C_6H_6)_2^+$ product decreases smoothly with increasing photon energy from 0.90 at $h\nu$ = 0.99 eV to 0.04 at 1.80 eV. The behavior is consistent with the following two-step model for the formation of $C_6H_6^+$. The photo-excited $(C_6H_6)_3^+$ ion first ejects one C_6H_6 molecule, yielding the transient dimer ion. If the dimer ion has sufficient internal energy, it further dissociates into $C_6H_6^+$ and C_6H_6. Statistical theories for unimolecular reactions are applied to predict the translational energies and the branching ratios. A comparison of the theoretical branching ratios with the experimental data suggests that a part (30-35%) of the product internal energy is distributed to the intramolecular vibrations of the extra C_6H_6 molecule. As far as the energy partitioning is concerned, the extra C_6H_6 molecule is no longer a spectator.

III-B-4 Photodissociation Spectroscopy of $(Benzene\text{-}Toluene)^+$. Charge Delocalization in the Hetero-Dimer Ion

Kazuhiko OHASHI *(Kyushu Univ. and IMS)*, **Youko NAKANE** *(Kyushu Univ.)*, **Yoshiya INOKUCHI, Yasuhiro NAKAI** *(Kyushu Univ.)* **and Nobuyuki NISHI**

[*Chem. Phys.* in press]

The electronic spectrum of the benzene-toluene hetero-dimer ion is measured in the 380-1400 nm region. The spectrum shows intense bands around 1175 and 670 nm and a weaker band around 920 nm, which correspond to charge resonance (CR) bands of homo-dimer ions. The observation indicates that the positive charge stays on the benzene part in some probability, although the ionization potential of benzene is 0.4162 eV higher than that of toluene. A local excitation (LE) band is observed around 420 nm, where a $\pi \leftarrow \pi$ transition is locally excited in the charged benzene or toluene molecule. On the basis of the positions of the CR-like bands as well as the intensity of the LE band relative to that of homo-dimer ions, the probability of finding the charge on the benzene molecule is analyzed to be approximately 36 %.

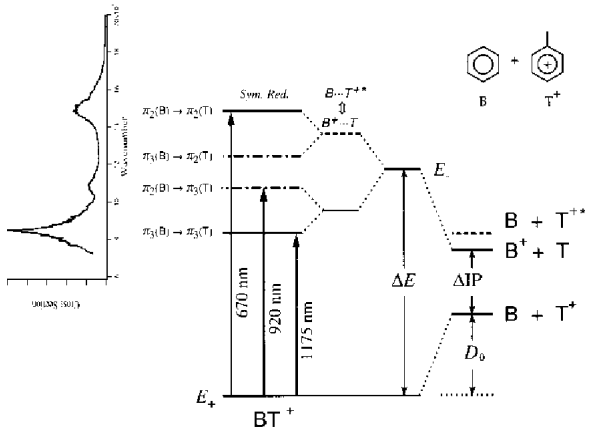

Figure 1. Energy level diagram for analyzing near-resonance interactions in BT^+. The $B^+ + T$ dissociation limit is located above the $B + T^+$ limit by ΔIP (0.4162 eV). The dissociation energy of BT^+ into $B + T^+$ is determined to be D_0 = 0.53 eV. Near-resonance interaction between $B\cdots T^*$ and $B^*\cdots T$ locates the hypothetical excited state 0.53 eV (= D_0) above the $B^+ + T$ limit. Near-resonance interaction between $B^+\cdots T$ and

$B\cdots T^{+}$*(a LE state correlating to the $B + T^{+}$* limit) makes the energy gap of the two excited states much wider. Each of the two states further splits into two levels due to the lift of the degeneracy (symmetry reduction) of $\pi_2(B)$ and $\pi_3(B)$. Although the energy difference (0.11 eV) between $B^+ + T$ and $B + T^{+}$* is neglected, the transition energy from the ground state to the hypothetical excited state ($\Delta E = 2D_0 + \Delta IP = 1.48$ eV) is in good agreement with the average (1.45 eV) of the transition energies observed for the 1175 and 670 nm bands. Main configurational changes of the SOMO electron upon the four types of excitations are also shown on the left side with the observed spectrum.

III-B-5 Photodissociation Spectrum of Cyanobenzene Dimer Cation. Absence of Intermolecular Resonance Interaction

Kazuhiko OHASHI *(Kyushu Univ. and IMS)*, **Masaharu NISHIGUCHI** *(Kyushu Univ. and IMS)*, **Yoshiya INOKUCHI, Hiroshi SEKIYA** *(Kyushu Univ.)* **and Nobuyuki NISHI**

[*Res. Chem. Intermed.* **24**, 755(1998)]

Electronic spectra of a homo-molecular dimer cation, $(C_6H_5CN)_2^+$, are measured by photodissociation spectroscopy in the gas phase. Broad feature appeared in the 450-650 nm region are characteristic of $\pi_3 \rightarrow \pi_{CN}$ transition of the $C_6H_5CN^+$ chromophore. No intense band is observed in the 650-1300 nm region, where other aromatic dimer cations show charge resonance bands. Two component molecules of $(C_6H_5CN)_2^+$ cannot take a parallel sandwich configuration suitable for the resonance interaction, because of geometrical constraints due to other stronger interactions.

III-C Ultrafast Dynamics of Photoexcited Molecules by Transient Absorption Spectroscopy

Ultrafast transient absorption spectroscopy is now an universal and popular method for the study of reaction pathways induced by electronic excitation of organic or metal complex molecules. Although we are going to introduce a new femto-pico synchronized multi-laser beam system in the coming spring, we have improved the specification of the old style dye amplifier system that will take a role of a complementary equipment particularly for the use of strong subpicosecond light source around 300 nm. This system is used for collaborative studies with organic chemists.

III-C-1 Construction of a Subpicosecond Time-Resolved Absorption Spectrometer Using a Dye Amplifier

Takakazu NAKABAYASHI and Nobuyuki NISHI

Although Ti:sapphire laser systems are widely used as ultrafast light sources, dye laser systems remain attractive sources because a tunable visible light with a high pulse energy cannot be easily obtained by using Ti:sapphire lasers at the present stage of development. We have thus constructed a subpicosecond time-resolved absorption system using an amplified dye laser, to the experiments for which visible light pulses are needed. A beam from a frequency-doubled cw mode-locked Nd:YAG laser is used to excite a synchronously pumped, hybridly mode-locked dye laser. Light pulses with 800 fs duration and 1 nJ pulse energies are obtained at a repetition rate of 76 MHz. The laser wavelength is tunable between 560 and 670 nm. Pulses from the dye laser pass through a dye amplifier, and amplified pulses with pulse energies of 1 mJ are obtained at a repetition rate of 10 Hz. The dye amplifier is excited by the second harmonic output from a pulsed Nd:YAG regenerative amplifier. The second-harmonic output of the dye amplifier is used as a pump beam, and the visible radiation that remained unconverted is focused into a cell containing water to generate a white light continuum. The generated continuum is split into two parts, one for a probe beam and the other for a reference. After passing through fixed (for the pump beam) and variable (for the probe beam) optical delay lines, the pump and probe beams are focused onto the sample cell. The continuum light intensities are detected by multichannel photodiodes and collected at a 10 Hz repetition rate synchronized with the light source. Time-resolved absorption spectra of some polyatomic molecules have been observed by using this spectrometer.

III-C-2 Time-Resolved Absorption Studies on Photochromism of 2H-Chromene Derivatives

Yoichi KODAMA *(Univ. Tsukuba and IMS)*, **Takakazu NAKABAYASHI, Nobuyuki NISHI and Hirochika SAKURAGI** *(Univ. Tsukuba)*

Spiropyrans being one of the most typical photochromic compounds have been extensively studied because they have potentially important applications as optoelectronic devices. Since these structures are too large to be analyzed quantitatively, little is known about reaction pathways in the photochromism of spiropyrans. We have therefore studied photoexcitation dynamics of 2H-chromenes (benzopyrans), which are simplified models of spiropyrans, by femto to microsecond time-resolved absorption spectroscopy. Figure 1 shows transient absorption changes of 2,4-diphenylchromene in various time regions. The transient absorption spectrum of 2,4-diphenylchromene (closed form) exhibit peaks at 390, 410, and 470 nm, all of which are attributed to the open form. The open form is shown to form within 2 ps and return to the closed form on the microsecond timescale. Four relaxation processes are observed with a time constant of 20 ps, 200 ps, 700 ns, and 50 μs, respectively. They are attributed to

vibrational relaxation (20 ps) and the lifetimes of three dynamically distinct open isomers (200 ps, 700 ns, 50 μs). The reaction mechanism describing the photochromism of 2H-chromenes is discussed on the basis of the observed results.

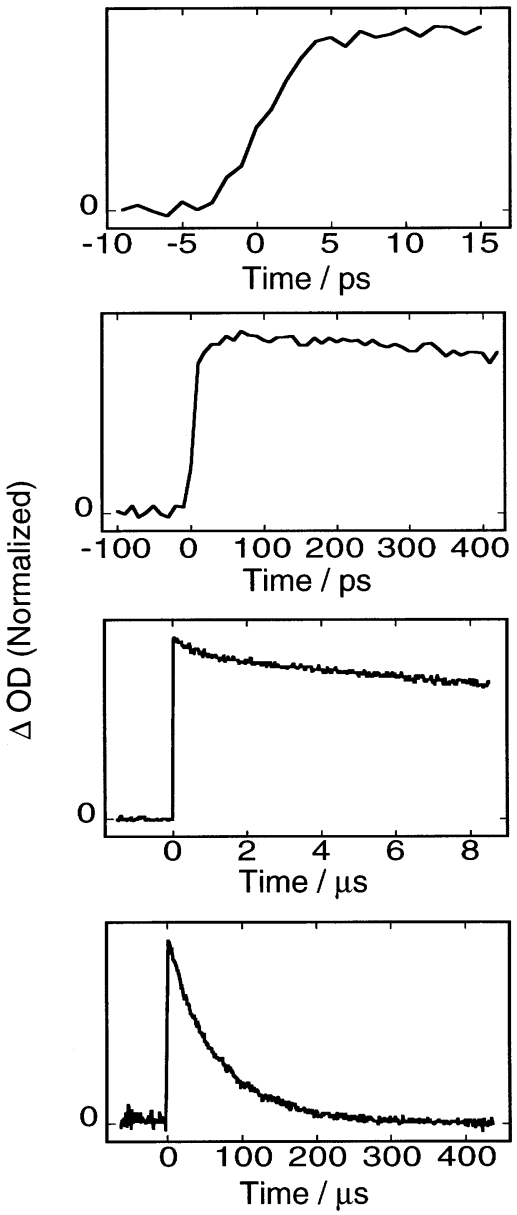

Figure 1. Transient absorption signals obtained from 2,4-diphenylchromene in cyclohexane in various time regions (probe, 400 nm).

III-D Photochemistry on Well-Defined Surfaces

Upon the irradiation of light in the wavelength range from visible to ultraviolet, a number of adsorbed molecules on metal surfaces reveal variety of photochemical processes, including photo-stimulated desorption, rearrangement of adsorbed states, photodissociation, and photo-initiated reactions with coadsorbates. A central and fundamental question in the surface photochemistry is to clarify how adsorbate-substrate systems are excited by photon irradiation. In addition, since photo-initiated reactions can be induced without any thermal activation of reactants, they may provide good opportunities for studying a new class of surface reactions which may not be induced thermally. We have studied photochemistry of various adsorption systems on well-defined metal and semiconductor surfaces mainly by temperature-programmed desorption (TPD), x-ray photoelectron spectroscopy (XPS), work function measurements, near edge x-ray absorption fine structure (NEXAFS) and angular-resolved time-of-flight (TOF) spectroscopy of photodesorbed species associated with pulsed laser irradiation. We have shown that methane weakly adsorbed on Pt(111) and Pd(111) is dissociated or desorbed by irradiation of 6.4-eV photons, which is far below the excitation energy for the first optically allowed transition of methane in the gas phase. In this year, we have started extensive investigations of photodesorption of rare gas atoms from semiconductor surfaces. This

physisorption system is very similar to methane on the transition metal surfaces in a sense that the photo-induced processes take place at the wavelengths where there is no absorption band in the gas phase.

III-D-1 Photodesorption of Xe Adsorbed on Clean and Oxidized Si(100) Surfaces

Kazuya WATANABE and Yoshiyasu MATSUMOTO

Rare gas weakly adsorbs on solid surfaces. The ionization potential is larger than typical polyatomic molecules and the first electronic excited state is also located at higher energy. Its electron affinity is negative. Thus, no photo-induced processes are expected under the irradiation of photon whose energy less than 6 eV. However, we have observed for the first time that Xe weakly adsorbed on clean and oxidized Si(100) surfaces is desorbed by the irradiation of photon with the energy ranging from 1.2 to 6.4 eV. Xe is adsorbed on the surfaces at 50 K. UV and visible photons are irradiated onto the surfaces. Post-irradiation TPD is observed as a function of irradiated photon numbers. The area of TPD peaks decreases with increase of the number of photons, indicating the coverage of Xe is reduced by the photon irradiation. Figure 1 shows that the TOF distributions of Xe photodesorbed by 6.4-eV photons. Thus, it is clear that Xe is desorbed by the photon irradiation. The TOF distribution of Xe from the clean Si(100) surface is well represented by Maxwell-Boltzmann distribution with a mean kinetic energy of 0.06 eV. On the other hand, the TOF distribution from the oxidized Si(100) surface shows multiple velocity components with mean kinetic energies of 0.8 eV and 0.3 eV. Those TOF distributions do not show any significant dependence on laser wavelength and fluence. Since Xe is weakly adsorbed on the surfaces, thermal heating by substrate photon absorption may induce desorption. However, the observed mean kinetic energies are all higher than the temperature attainable by the photon irradiation. Furthermore, if the thermal heating is a true origin of the desorption, the TOF distribution should depend on the laser fluence. However, the observed results are not consistent with these expectations. Thus, the Xe desorption from these surfaces are not simply induced by thermal heating by photon irradiation. In order to clarify the excitation mechanism, we will measure more carefully the wavelength dependence of effective cross sections and TOF distributions.

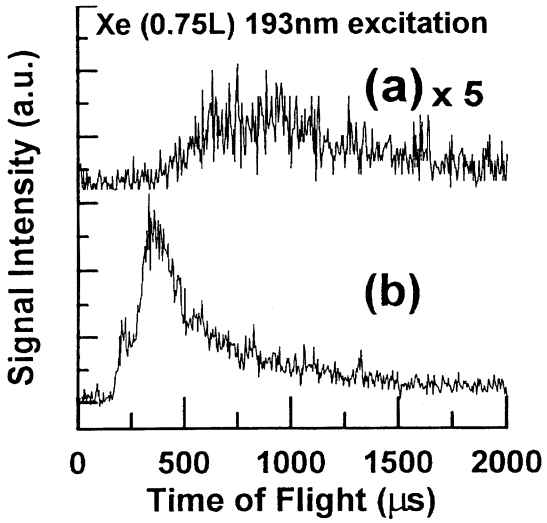

Figure 1. Time-of-flight distributions of Xe desorbed from (a) a clean Si(100) and (b) an oxidized Si(100). The surfaces are irradiated by 6.4 eV (193 nm) excimer laser pulses.

III-E Photochemistry of Adsorbates on Thin Films and Clusters of Metals

An isolated atom has a set of discrete energy levels. On the other hand, as a result of mutual interactions of atoms, the electronic structure of a bulk solid is composed of a set of energy bands. Ultra-thin films and microclusters provide a unique opportunity for studying how the electronic structure changes from one to the other. In such nano-structured materials electronic levels are still discrete and photo-induced energetic electrons likely show ballistic motions rather than stochastic ones. Thus, they may show unique electronic properties and chemical reactivities. We have concentrated on how molecules interact with bulk metal surfaces and how they are excited by photons as described in the previous section. From this year we have started a project to study how the electronic properties and reactivities depend on the size and thickness of the spatially confined systems; these are more relevant to real world chemistry, i.e. catalysis.

III-E-1 Photochemistry of Methane adsorbed on Pd/Al_2O_3 Model Catalysts

Kazuo WATANABE, Margarethe KAMPLING *(Fritz-Haber-Institut der Max-Planck-Gesellschaft)***, Katharina AL-SHAMERY** *(Fritz-Haber-Institut der Max-Planck-Gesellschaft)***, Hans-Jochaim FREUND** *(Fritz-Haber-Institut der Max-Planck-Gesellschaft)* **and Yoshiyasu MATSUMOTO**

Conversion of methane into useful chemical reagents has been extensively studied for several decades owing to the increasing industrial and environmental importance. However, methane is the most stable hydrocarbon and the previous efforts to break the methane C-H bond thermally have not necessary been successful regarding the efficiency and costs even with sophisticated catalysts. Recently, we have discovered that methane physisorbed on Pt(111) and Pd(111) surfaces is photodissociated into methyl

and hydrogen by 193-nm (6.4 eV) ArF excimer laser irradiation despite gaseous methane is transparent at this wavelength.[1)] The electronic interaction between methane and metal surfaces in the unoccupied states plays an important role in this photoexcitation. To further investigate the mechanism of this new photochemistry, we study adsorption states and photoreactions of methane adsorbed on Pd clusters deposited on thin Al_2O_3 films on a NiAl(110) substrate. Depending on the size and the structure of Pd-clusters, the strength of interaction between methane and Pd-clusters changes significantly, and consequently the photoreaction cross section and the branching ratios of reaction (photodissociation/photodesorption) change dramatically.

Reference

1) Y.Matsumoto, Y.A.Gruzdkov, K.Watanabe and K.Sawabe, *J. Chem. Phys.* **105**, 4775 (1996).

III-F Reaction Dynamics on Well-Defined Surfaces

Vast majority of surface reactions studied so far has been interpreted in terms of a Langmuir-Hinshelwood mechanism; reactants are first adsorbed on a surface and a reaction takes place between two chemisorbed species. Although reactants are in equilibrium with surface atoms, the energetics of desorbed products are determined by potential energy surfaces along reaction coordinates. In particular, associative desorption, which is often a reversed process of activated dissociative chemisorption, shows interesting features manifested by a potential barrier near the exit channel. In this year, we have made an extensive study of CO_2 conversion to carbonate on Si(100) coadsorbed with N_2O and O_2.

III-F-1 Effective Conversion of CO_2 to Carbonate in Surface Oxidation Processes at Si(100)

Kazuya WATANABE, Hiroyuki KATO *(Grad.Univ. Adv. Stud.)* **and Yoshiyasu MATSUMOTO**

[*J. Phys. Chem.* in press]

It is found that effective carbonate formation occurs at a clean Si(100) surface between CO_2 and surface oxidants: N_2O and O_2. The reactions of CO_2 with N_2O or O_2 are studied by temperature-programmed desorption and X-ray photoelectron spectroscopy. CO_2 physisorbed on Si(100) desorbs exclusively at (75 K. However, when CO_2 is coadsorbed with N_2O or O_2, CO_2 is converted very effectively into surface carbonate species below 140 K. The carbonate species are dissociated to produce desorbed species of CO or CO_2 in the temperature range of 200-600 K. By using $C^{18}O_2$, it is confirmed that the carbonate is composed of the adsorbate CO_2 and one oxygen atom from the surface oxidant. In the case of N_2O/CO_2 coadsorption, the carbonate formation is mainly induced by thermal dissociation of N_2O adsorbates. In the case of O_2/CO_2 coadsorption, the carbonate formation is not only induced by dissociative chemisorption of O_2, but also proceeded with chemisorbed dioxygen that likely adsorbs in a peroxy bridging configuration.

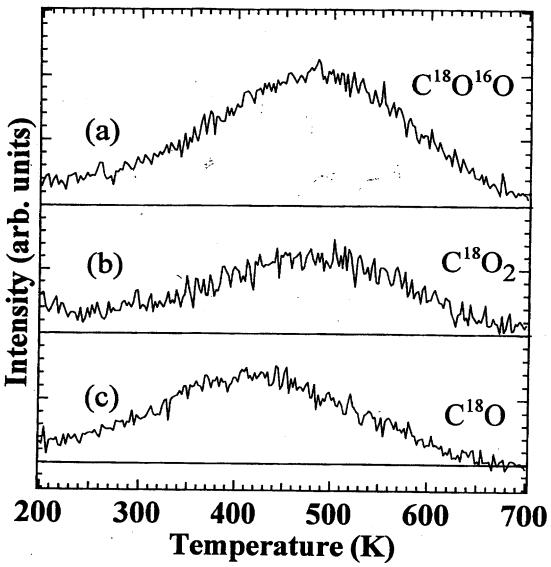

Figure 1. TPD results measured at (a) m/e=46 ($C^{18}O^{16}O$), (b) m/e=48 ($C^{18}O_2$), and (c) m/e=30 ($C^{18}O$) taken from Si(100) exposed to CO_2 (0.4 L) and O_2 (1.0 L). The surface was first exposed to CO_2 and then to O_2. The heating rate was 4.0 K/s.

III-G Dynamical Behavior of Electronically Excited States

Understanding the dynamics of photoexcited dye molecules in solution, such as the intra- and intermolecular vibrational energy relaxation, solvation dynamics and electron transfer reaction, has been an area of intense research in recent years. If the excited molecules have an excess vibrational energy, vibrational relaxation should affect the spectral evolution of the solvation dynamics within a few picosecond time scale. We investigated the internal conversion (IC) and intramolecular vibrational energy redistribution process (IVR) of coumarin 481 (C481) in solutions with a large excess energy in order to reveal how the vibrational relaxation is coupled to the solvation process.

III-G-1 Ultrafast Relaxation Processes from a Higher Electronically Excited State of a Dye Molecule in Solution: A Femtosecond Time-Resolved Fluorescence Study

Kaoru OHTA *(Kyoto Univ. and IMS)*, **Tai Jong KANG** *(Taegu Univ. and IMS)*, **Keisuke TOMINAGA and Keitaro YOSHIHARA** *(JAIST)*

[*Chem. Phys.* submitted]

We have investigated the internal conversion, intramolecular energy redistribution, and vibrational cooling of coumarin 481 in cyclohexane after the photoexcitation by a third harmonic of the Ti:Sapphire laser (267 nm). Following the photoexcitation to a higher electronic state, we observe the fluorescence up-conversion signals at several wavelengths. The experimental results show that the fluorescence signals rise with time constants of 220-280 fs at all the wavelengths, and these is no drastic change of the spectral shape within a few picoseconds. These suggest that the observed dynamics are mainly due to the internal conversion from the S_n to S_1 state and the intramolecular energy redistribution takes place much faster than the former process. We also perform the model calculation of the fluorescence spectrum by assuming three Franck-Condon active modes to obtain information on the relaxation process. A spectral change due to vibrational cooling is observed in a time scale of 10 ps, which is simulated quite well in terms of the thermal diffusion equation.

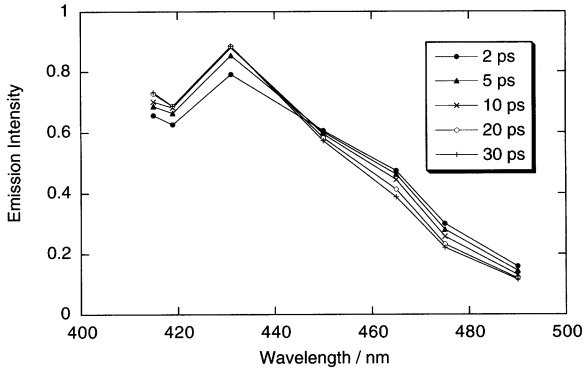

Figure 1. Time-resolved fluorescence spectrum of coumarin 481 excited at 267 nm in cyclohexane.

III-H Spectroscopy and Dynamics of Vibrationally Excited Molecules and Clusters

This research group, which started in April 1997, is planning to study spectroscopy and dynamics of molecules and clusters in higher vibrational state by two-color double resonance spectroscopy. New spectroscopic methods will also be developed to observe the higher vibrational state under collision-free condition.

III-H-1 Nonresonant Ionization Detected IR Spectrum of Jet-Cooled Phenol — Ionization Mechanism and Its Application to Overtone Spectroscopy

Shun-ichi ISHIUCHI *(Grad. School. Waseda Univ.)*, **Hiroshi SHITOMI** *(Grad. School Waseda Univ.)*, **Ken TAKAZAWA** *(National Research Institute for Metals)* **and Masaaki FUJII**

[*Chem. Phys. Lett.* **283**, 243 (1998)]

Vibrational transitions of jet-cooled phenol have been detected by nonresonant two-photon ionization due to UV laser from 3400 cm^{-1} to 14000 cm^{-1}. The UV frequency dependence of IR-UV double resonance signals is used for discussion on the mechanism of ionization. The spectrum shows a well-resolved structure due to the first to the fourth quantum of OH stretching vibrations, CH overtones and various combination vibrations. The vibrational frequency, anharmonisity and the dissociation energy of the OH stretching mode has been measured. The bandwidth of the OH overtone is found to decrease with increase in the vibrational quantum number.

III-H-2 Structure of 1-Naphthol-Water Clusters Studied by IR Dip Spectroscopy and Ab Initio Molecular Orbital Calculation

Ruriko YOSHINO *(Grad. School. Waseda Univ.)*, **Kenro HASHIMOTO** *(Tokyo Metropolitan Univ.)*, **Takuichiro OMI** *(Grad. School. Waseda Univ.)*, **Shun-ichi ISHIUCHI** *(Grad. Univ. Adv. Stud.)* **and Masaaki FUJII**

[*J. Phys. Chem. A* **102**, 6227-6233 (1998)]

IR spectrum of cis-1-naphthol, trans-1-naphthol, and 1-naphthol·$(H_2O)_n$ (n = 1-3) clusters has been measured by the IR dip spectroscopy in a supersonic jet. The spectra show clear vibrational structures of the monomers and the clusters in the energy region from 3000 cm^{-1} to 3800 cm^{-1}. Observed vibrational transitions are assigned to the OH stretching vibrations of 1-naphthol and waters in the clusters. The size dependence of the IR bands and the cluster geometries are analyzed by using the ab initio MO method at MP2/6-31G level. From the comparison between the observed and calculated IR spectra, we have concluded that the 1-naphthol acts as the proton donor and a cyclic hydrogen-bond network is formed in the n = 2 and 3 clusters.

III-I Large Amplitude Motion in Molecular Cation Studied by Pulsed Field Ionization - Zero Kinetic Energy Photoelectron Spectroscopy

Large amplitude motion is important subject in spectroscopy, and is a fundamental model to understand nonrigid motion in biological systems and that in chemical reaction. In this project, large amplitude motion, such as internal rotation, intermolecular vibration in cation radicals will be observed by using PFI-ZEKE photoelectron spectroscopy, and its change by ionization will be discussed.

III-I-1 Internal Rotation of Methyl Group in Tolunitrile Cations Studied by Pulsed Field Ionization - Zero Kinetic Energy Spectroscopy

Kazunari SUZUKI *(Grad. School Waseda Univ.)*, **Keigo YOSHIDA** *(Grad. School Waseda Univ.)*, **Yuji EMURA** *(Grad. School Waseda Univ.)*, **Hideyuki IKOMA** *(Grad. School Waseda Univ.)* **and Masaaki FUJII**

Pulsed Field Ionization-Zero Kinetic Energy (PFI-ZEKE) photoelectron spectroscopy has been applied to *o*-, *m*- and *p*- tolunitrile in a supersonic jet. The PFI-ZEKE spectra of *m*- and *p*-tolunitrile show well-resolved structure due to internal rotation of the methyl group in the corresponding cations. Level energies and transition intensities were reproduced by a one-dimensional rotor model with a free-rotor basis set, and the potential curves of the internal rotation in the cations have been determined. Analysis for *m*- and *p*-tolunitrile shows a slight increase of the barrier height for internal rotational motion from the neutral to the corresponding cation. On the other hand, no internal rotational bands was found in the PFI-ZEKE spectrum of *o*-tolunitrile. It suggests that ionization does not cause the significant change of the barrier height for the internal rotation in *o*-tolunitrile. This tendency is largely different from other toluene derivatives, such as toluidine,[1)] which shows the drastic increase of the internal rotational barrier after ionization. The substituent effect on the internal rotational motion has been discussed.

Reference

1) H. IKOMA, K. TAKAZAWA, Y. EMURA, S. IKEDA, H. ABE, H. HAYASHI and M. FUJII, *J. Chem. Phys.* **105**, 10201 (1996).

III-J Laser Investigation of Molecular Photodissociation Dynamics

Detailed studies on photodissociation dynamics provides the basis for understanding molecular photochemistry and bimolecular reactions (full collisions). This project aims at, (1) the development of new experimental techniques to obtain complete information on quantum state distributions of reaction products, and (2) the elucidation of complex dissociation dynamics of polyatomic molecules. Lasers with high intensity, good monochromaticity, and well-defined polarization provide extremely sensitive detection methods of reaction products with the capability of examining their scalar (e.g. energy) and vector (e.g. linear and angular momenta) quantities. The extensive use of laser-based techniques is the key for the elucidation of complicated dynamics. Our major effort have been directed to the development of two and three dimensional imaging techniques to visualize the scattering of atoms and molecules and also the development of theoretical treatment of vector correlation observed in imaging. By coupling the laser and imaging techniques, differential cross section can be measured with complete internal state selection.

III-J-1 Quantal and Semiclassical Analysis of Vector Correlation in Molecular Photodissociation

Yuxiang MO and Toshinori SUZUKI

[*J. Chem. Phys.* **108**, 6780 (1998)]

General semiclassical expressions for state multipoles and multipole moments have been obtained by the correspondence principle. The expression derived for low-rank multipole moments is identical with that obtained by comparing quantal and classical formulae for one- and two-photon absorption intensity of diatomic molecules. [D. A. Case, G. M. McClelland and D. R. Herschbach, *Mol. Phys.* **35**, 541 (1978)]. For molecular photodissociation, *quantal* expressions for multipole moments have been obtained by formal expansion of the density matrix by the state multipoles of fragment angular momentum both in the *velocity-fixed* (*VF*) and the *transition dipole moment fixed* (μF) frames. The formulae derived in the two frames were proved to be equivalent. Semiclassical formulae have been also obtained in *VF* and μF frames by approximating the quantal multipole moments with the *semiclassical expressions*. The expression thus obtained in the μF frame is in agreement with that reported by Dixon [*J. Chem. Phys.* **85**, 1866 (1986)].

III-J-2 Geometrical Factors of Two-Photon Absorption for the Determination of Alignment and Orientation

Yuxiang MO and Toshinori SUZUKI

[*J. Chem. Phys.* **109**, 4691 (1998)]

It is shown that the relative ratios of geometrical factors in two-photon transition are invariant to the character of the virtual states and are expressed by a simple formula for both linearly and circularly polarized light. The recognition of this simple relation would much simplify the analysis of polarization dependence of signal intensity observed.

III-J-3 Probing alignment of NO($X^2\Pi$) by [2+1] REMPI via C $^2\Pi$ state: A Test of Semiclassical Theory in 355 nm Photodissociation of NO_2

Yuxiang MO, Hideki KATAYANAGI and Toshinori SUZUKI

[*J. Chem. Phys.* in press]

A theoretical method is presented to analyze 2D and 3D imaging data of photofragments with polarized angular momentum. The theory is critically tested by comparison with the experimental data on NO from 355 nm photodissociation of NO_2. The alignment of NO($X^2\Pi$) is detected by [2+1] resonance-enhanced multiphoton ionization (REMPI) via the C $^2\Pi$ state. The angular momentum polarization of NO is described by semiclassical multipole moments expressed by vector correlation in the *velocity-fixed* frame. The geometrical factors for two-photon absorption, P_k, are derived rigorously for the intermediate coupling between Hund's cases (a) and (b), however, it is also shown that the factors for large angular momenta are independent of the coupling case and approximated by simple formulae. Excellent agreement of simulation with the experimental data proves the validity of the theory.

III-J-4 Non-Adiabatic Bending Dissociation in 16 Valence Electron System OCS

Toshinori SUZUKI, Hideki KATAYANAGI, Shinkoh NANBU and Mutsumi AOYAGI

[*J. Chem. Phys.* **109**, 5778 (1998)]

The speed, angular and alignment distributions of S($^1D_2$) atoms from the ultraviolet photodissociation of OCS has been measured by a photofragment imaging technique. From the excitation wavelength dependence of the scattering distribution of S($^1D_2$), the excited states accessed by photoabsorption were assigned to the A' Renner-Teller component of the $^1\Delta$ and the A"($^1\Sigma^-$) states. It was found that the dissociation from the A' state gives rise to high and low-speed fragments, while the A" state only provides the high-speed fragment. In order to elucidate the dissociation dynamics, in particular the bimodal speed distribution of S atoms, two-dimensional potential energy surfaces of OCS were calculated for the C-S stretch and bending coordinates by ab initio method (MCSCF/SDCI/DZP). Conical intersections of $^1\Delta$ and $^1\Sigma^-$ with $^1\Pi$ were found as adiabatic dissociation pathways. Wave packet calculations on these adiabatic surfaces, however, did not reproduce the low-speed component of S($^1D_2$) fragments. The discrepancy regarding the slow S atoms was attributed to the dissociation induced by non-adiabatic transition from A'($^1\Delta$) to A'($^1\Sigma^+$) in the bending coordinate. This hypothesis was confirmed by wave packet calculations including non-adiabatic transitions. The slow recoil speed of S atoms in the non-adiabatic dissociation channel is due to more efficient conversion of bending energy into CO rotation than the adiabatic dissociation on the upper state surface. By analyzing the experimental data, taking into account the alignment of S($^1D_2$) atoms, we determined the yield of the non-adiabatic transition from the A'($^1\Delta$) to the ground states to be 0.31 in the dissociation at 223 nm. Our theoretical model has predicted a prominent structure in the absorption spectrum due to a Feshbach resonance in dissociation, while an action spectrum of jet-cooled OCS measured by monitoring S($^1D_2$) exhibited only broad structure, indicating the limitation of our model calculations.

III-J-5 C-Br Bond Rupture in 193 nm Photodissociation of Vinyl Bromide

Hideki KATAYANAGI, Nobuaki YONEKURA and Toshinori SUZUKI

[*Chem. Phys.* **231**, 345 (1998)]

Photofragment ion imaging has been applied to 193 nm photodissociation of vinyl bromide to measure the speed and angular distributions of Br atoms. Br atoms were observed in both spin-orbit states (^2P_J; J= 1/2 or 3/2) with the branching ratio, [Br*]/[Br], of 0.06 ± 0.03. Both Br(^2P_J) distributions were dominated by anisotropic high translational energy components, which are ascribed to C-Br bond rupture via surface crossing between the optically-excited $^1(\pi,\pi^*)$ state and ^{1}(n(Br) or π(Br), σ^*(C-Br)) repulsive state(s). The anisotropy parameters of the high translational energy components, 1.3 (Br) and 1.2 (Br*), provide the direction of the transition dipole moment for the $\pi^* \leftarrow \pi$ transition to be 26 ± 3° from the C=C bond axis, in good agreement with ab initio calculations by Yamashita. Despite that the available energy is 10.5 kcal/mol smaller in the Br* channel, the peak energies of P(E_T) in the Br* and Br channels were quite similar, indicating that the fine structure branching occurs in the molecular region. Low translational energy components of Br and Br* observed are ascribed to the dissociation of VBr from the ground state, although contribution from the secondary dissociation of C_2H_2Br radical is also suggested for the Br channel. The anisotropy of low energy component implies that the lifetime of the ground state VBr is only a fraction of its rotational period.

III-J-6 Energy Barrier for the C-C Bond Rupture in Acetyl Radical Studied by Nanosecond Photofragment Imaging

Hideki KATAYANAGI and Toshinori SUZUKI

[*J. Chem. Phys.* in press (1998)]

Nanosecond photofragment imaging has been applied to UV photodissociation of acetyl chloride. From the scattering distributions of acetyl radical, the energy barrier for the C-C bond rupture in acetyl radical was estimated to be 14.5 ± 1 kcal/mol.

III-J-7 Dissociation of Metastable CH_3CO Radical Observed by Subpicosecond Time-Clocked Imaging

Takeshi SHIBATA *(Grad. Univ. Adv. Stud.)*, **Haiyang LI, Hideki KATAYANAGI and Toshinori SUZUKI**

[*J. Phys. Chem. A* **102**, 3643 (1998)]

A novel experimental technique to measure the energy-dependent unimolecular dissociation rate k(E) of radical species is presented. Internally-excited CH_3CO radicals were formed by ultraviolet photodissociation of CH_3COCl, and the subsequent decay of these radicals were detected by subpicosecond time-clocked photofragment imaging. The CH_3CO radicals with different internal energies were dispersed in space by their recoil velocities, and their decay rates were measured for each internal energy. The dissociation rates of CH_3CO radicals determined were an order of magnitude smaller than those calculated by Rice-Ramsperger-Kassel-Marcus theory.

III-J-8 Sensitized Phosphorescence Detection of Metastable Triplet Acetylene Produced by Intersystem Crossing

Yang SHI and Toshinori SUZUKI

[*J. Phys. Chem. A* **102**, 7414 (1998)]

The triplet metastable states of acetylene produced by intersystem crossing from the $\tilde{A}(^1A_u)$ state have been detected by sensitized phosphorescence (SP) method. The phosphorescence was observed in the energy region up to V^4K^2 level that is below the barrier to dissociation in the $\tilde{a}$ state suggested previously. The lifetimes of the triplet states coupled with the V^3K^1 and V^4K^1 levels in the were estimated to be 80 and 100 μs. The rotational structures of SP and LIF spectra were similar, except that weak absorption lines appear more strongly in SP spectrum, thus making SP spectrum more congested. This exemplifies complicated singlet-triplet mixing at the V^3K^1 level suggested previously. The SP signal was observed with different phosphors, where benzil provided the most intense SP signal. Using benzil, the SP spectrum was also be measured for C_2D_2. The prompt emission from Acetylene in collision with the surface was observed for all the phosphors, which is most likely to be due to intersystem crossing from the triplet to the $\tilde{A}(^1A_u)$ state. The lifetime of triplet states and the threshold energy for dissociation for C_2H_2 and C_2D_2 suggest that there is a tunneling effect in dissociation in the triplet manifold.

III-J-9 Predissociation of Acetylene from the $\tilde{A}(^1A_u)$ State Studied by Absorption, LIF and H-Atom Action Spectroscopies

Nobuhisa HASHIMOTO and Toshinori SUZUKI

[*J. Chem. Phys.* in press]

The state dependence of the fluorescence quantum yield and predissociation yield of acetylene in the $\tilde{A}$ state have been investigated. The fluorescence quantum yield decreased with the total angular momentum J at the V^3K^1 and V^4K^1 levels, while not at V^2K^1. Dissociation yield from the V^4K^1, V^5K^1, and V^6K^1 did not depend upon J. The absolute fluorescence quantum yield was found to be only 0.02 at the V^4K^1 J' = 2 level, and more surprisingly 0.13 even at the V^2K^1 J' = 2 level located 1778 cm^{-1} below the dissociation threshold to C_2H ($\tilde{X}\ ^2\Sigma^+$) + H(^{2}S). The translational energy release determined from the Doppler line shape of H atoms suggests that dissociation mainly occurs in the $\tilde{a}$ state over the barrier. Although the singlet-triplet coupling has been believed to be mediated by the $\tilde{c}$ state, the absolute fluorescence quantum yield indicates that electronic relaxation is not specific for the levels lying close to the surface crossing point between the $\tilde{A}$ and $\tilde{c}$ states. It is suggested that internal conversion also plays a role in relaxation from the $\tilde{A}$ state and the ratio of internal conversion and intersystem crossing varies as a function of energy.

III-K Laser Investigation of Bimolecular Reaction Dynamics

In order to understand chemical reactions, detailed knowledge of the dynamics of atomic and molecular collisions is needed. Crossed molecular beams provide a powerful and versatile approach for the study of reactive and inelastic encounters. However, with the conventional detection technique using electron impact ionization, differential cross sections were hardly measured with rotational resolution. This project aims at the measurement of fully state-resolved differential cross sections for reactive scattering processes via two-dimensional ion imaging. The reaction of O($^1D_2$) atoms will be investigated because of their importance in atmospheric chemistry.

III-K-1 High-Resolution Measurements of State-Resolved Differential Cross Sections in NO + Ar Inelastic Scattering at E_{coll} = 65 meV

Hiroshi KOHGUCHI, Christian GEBAUER and Toshinori SUZUKI

We have constructed a crossed molecular beam machine with a 2D ion imaging detector. Each of the two beam sources are pumped by two diffusion pumps

(2 × 2000 l/s) backed by roots blowers (250 and 500 m^3/h), while the main chamber is pumped by tandem turbo molecular pumps (1500 l/s and 500 l/s). Two pulsed supersonic beams generated by piezoelectric valves are crossed at the right angle 50 mm downstream from the nozzles, and the scattered products are interrogated by a probe laser by resonance-enhanced multiphoton ionization. The subsequent ions are accelerated by an electric field in the direction perpendicular to the relative velocity vector and projected onto a gated two-dimensional position sensitive ion detector. The angular and speed distributions of the state-selected products are observed. An acceleration field has 2-D space focusing effect, and a hexapole deflector located in the drift region compensate the center-of-mass velocity of the particles to direct them to the center of the detector. The image observed by a video-rate CCD camera is processed in real time to calculate the center of the light spot on the screen for resolution enhancement. In order to evaluate the performance of the apparatus, inelastic scattering of NO (J" = 1/2, Ω" = 1/2) + Ar → NO (J', Ω' = 1/2, 3/2) was measured at the collision energy of 65 meV. Rotationally and spin-orbit excited NO were detected by $A^2\sum$-$X^2\prod$ [1+1] REMPI. Scattering images showed the state-dependent rotational rainbow peaks.

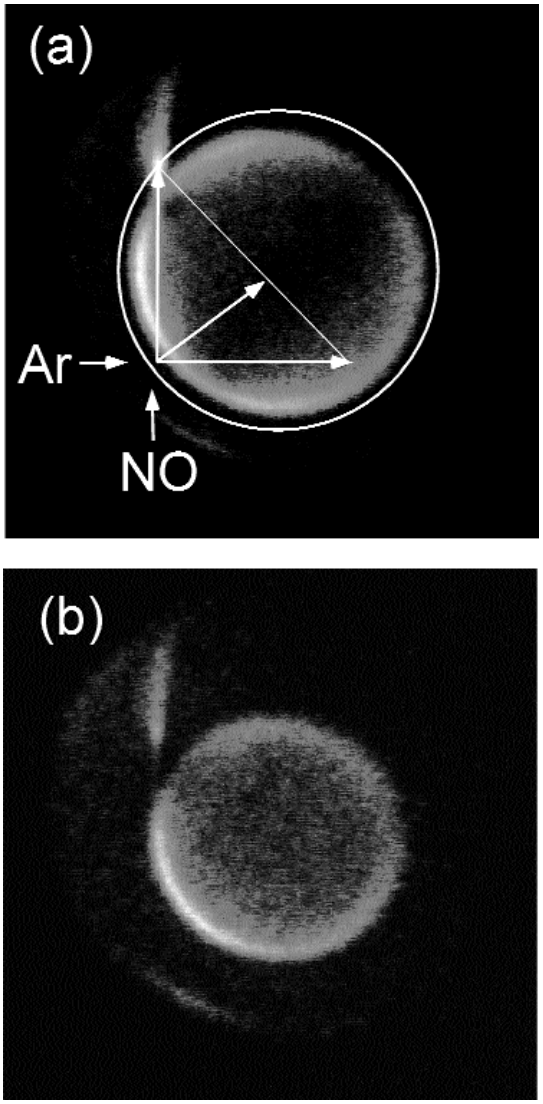

Figure 1. Two-dimensional images of NO scattered by Ar, a) Ω' = 1/2, v' = 0, J' = 8.5, and b) Ω' = 3/2, v' = 0, J' = 8.5. A Newton circle for elastic scattering limit is imposed. The images were integrated for 90 000 laser shots (60 minutes) each.

III-K-2 Development of an Intense Atomic Beam Source of O(^{1}D)

Hiroshi KOHGUCHI, Christian GEBAUER and Toshinori SUZUKI

The reactions of O(^{1}D) have large cross sections and play important roles in combustion or atmospheric chemistry. In order to study the O(^{1}D) reactions at the state-resolved differential cross section level, an intense atomic beam source of O(^{1}D) was developed. O(^{1}D) was produced by laser photolysis of O_2 molecule via Schumann-Runge band at 157nm (F_2 excimer laser, 50mJ/pulse). The intensity of the O(^{1}D) beam at the interaction region was monitored by VUV-LIF using the transition (2p O(^{1}D) → 3s O(^{1}D)) at 115.2 nm. The VUV light was generated by tripling the second harmonic of the output of a YAG-pumped dye laser. A high stagnation pressure up to 9 atm was used to confine the photolytically-generated O(^{1}D) atoms with fast recoil velocity (2200 m/s) in the molecular beam. Hellium was used as a career gas for its small quenching rate of O(^{1}D)+He → O(^{3}P)+He. Although the absolute concentration of O(^{1}D) was not deduced, the comparison with the B-X band (105.1nm) of CO indicated that the number density of O(^{1}D) is 5% of that of CO beam (5% CO/He) at the collision region.

III-L Spectroscopy and Excited State Dynamics in van der Waals Complexes

Spectroscopy and excited state dynamics in van der Waals complexes give much helpful information on the atom-molecule collision processes. We have studied two systems; 1) rare gas-NO system , which concerns with the collisional relaxation of excited NO molecule with rare gas and 2) N_2O-saturated hydrocarbon system (RH), in which $O(^1D)$ is produced in the photolysis of N_2O and the half-reactions of $O(^1D)$- RH are studied.

III-L-1 Electronic Spectroscopy and Predissociation Mechanism of Ar-NO in the 3p Rydberg States

Kazuhide TSUJI, Kosuke AIUCHI, Kazuhiko SHIBUYA *(Tokyo Inst. Tech.)* **and Kinichi OBI** *(Tokyo Inst. Tech. and IMS)*

[*Chem. Phys.* **231**, 279 (1998)]

The $\tilde{D}$ state was found to have surprisingly large D_0 values of l044 cm^{-1} for $v'_{NO} = 0$ and l004 cm^{-1} for $v'_{NO} = 1$, which are larger than 940 cm^{-1} of Ar-NO^+. From the analysis of these spectra, it was found Ar-NO in the 3p Rydberg states predissociates into NO and Ar at different rates strongly depending on the Rydberg orbital character, the vibrational quantum number (v'_{NO}) of NO moiety, and the intermolecular stretching quantum number (v'_{str}) of Ar-NO. Especially, the interaction of the 3p Rydberg states with the nearest-neighboring $\tilde{B}$ state plays an important role in these v'_{NO}- and v'_{str}- dependent predissociation of Ar-NO $\tilde{C}$ ($v'_{NO} = 0, 1, 2$) and ($v'_{NO} = 0, 1$).

III-L-2 Photochemical Reaction Dynamics of $O(^1D)$ with Saturated Hydrocarbons, CH_4, C_2H_6, and C_3H_8, under Bulk Conditions and in van der Waals Complexes

Shin-ichi WADA *(Tokyo Inst. Tech.)* **and Kinichi OBI** *(Tokyo Inst. Tech. and IMS)*

[*J. Phys. Chem. A* **102**, 3481, (1998)]

The reactions of $O(^1D)$ atom with saturated hydrocarbons (RH), CH_4, C_2H_6, and C_3H_8, were studied by monitoring the laser induced fluorescence of products OH in the $v'' = 0$ and 1 levels under bulk conditions and in van der Waals complexes, N_2O-RH. $O(^1D)$ was produced by the ArF excimer laser photolysis of N_2O. Nascent rotational distributions are bimodal in all cases; the low- and high-N components. The former is formed from a long-lived collision complex generated by the insertion process. The collision complex has enough lifetime to randomize excess energy before decomposition. The high-N component is produced in the short-lived insertion process, in which the collision energy of $O(^1D)$ atoms is reflected in the rotational energy. The spin-orbit state in the only half-reactions producing the $v'' = 0$ level shows large population in the low-lying $^2\prod_{3/2}$ state in low-N components, though spin-orbit populations are statistical in other reaction systems studied. The reaction proceeds via a transfer from a singlet reaction surface to a triplet surface keeping the conservation of the electronic angular momentum.

III-M Photochemical Processes Studied by Time-Resolved ESR

Photochemical processes generate abnormal electron spin polarization on excited molecules and free radicals, which is called as chemically induced dynamic electron spin polarization (CIDEP). We have studied photochemical reactions by probing CIDEP. We investigated the interaction in radical and triplet pairs and confirmed evidences for CIDEP generations by level crossing in triplet doublet interactions. Secondly, we succeeded in detection of singlet oxygen molecules by monitoring spin polarization generated on free radicals in the singlet oxygen-free radical systems.

III-M-1 Exchange Interaction in Radical-Triplet Pair: Evidence for CIDEP Generation by Level Crossings in Triplet-Doublet Interactions

Yasuhiro KOBORI *(Tohoku Univ.)***, Keizo TAKEDA** *(IBM)***, Kazuhide TSUJI, Akio KAWAI** *(Tokyo Inst. Tech.)* **and Kinichi OBI** *(Tokyo Inst. Tech. and IMS)*

Chemically induced dynamic electron polarization (CIDEP) generated through interaction of the excited triplet state of 1-chloronaphthalene, benzophenone, benzil, and Buckminsterfullerene (C_{60}) with 2,2,6,6 -tetramethyl-1-piperidinyloxyl (TEMPO) radical was investigated by using time-resolved ESR spectroscopy. We carefully examined what factors affect the CIDEP intensities. By comparing CIDEP intensities of TEMPO in the 1-chloronaphthalene, benzophenone, and benzil systems with that obtained in the C_{60}-TEMPO system, the absolute magnitude of net emissive polarization was determined to be -2.2, -6.9, and -8.0, respectively, in the units of Boltzmann polarization. In the 1-chloronaphthalene-TEMPO system, the viscosity effect on the magnitude of net polarization was studied by changing the temperature (226-275 K) in 2-propanol. The emissive polarization was concluded to result from the state mixing between quartet and doublet manifolds in a radical-triplet pair induced by the zero-field splitting interaction of the counter triplet molecule. The

magnitude of net polarization is much larger than the polarization calculated with the reported theory that CIDEP is predominantly generated in the region where the exchange interaction is smaller than the Zeeman energy. Our experimental results are quantitatively explained by the theory that CIDEP is generated predominantly in the regions where the quartet and doublet levels cross. We propose a theoretical treatment to calculate the magnitude of net polarization generated by the level crossings in the radical-triplet pair mechanism under highly viscous conditions and perform a numerical analysis of the net RTPM polarization with the stochastic-Liouville equation. The viscosity dependence of the net polarization indicates that the back transition from the doublet to quartet states sufficiently occurs in the level-crossing region under highly viscous conditions. The estimated large exchange interaction suggests that the quenching of the excited triplet molecules by TEMPO proceeds via the electron exchange interaction.

III-M-2 CIDEP in Radical-Singlet Molecular Oxygen System

Akio KAWAI *(Tokyo Inst. Tech.)*, **Masaaki MITSUI** *(Kyoto Univ.)*, **Yasuhiro KOBORI** *(Tohoku Univ.)* **and Kinichi OBI** *(Tokyo Inst. Tech. and IMS)*

[*Appl. Magn. Reson.* **12**, 405, (1997)]

Net absorptive CIDEP generation has been demonstrated on singlet molecular oxygen and 4-oxo-2,2,6,6-tetramethyl-1-piperidinyloxyl (OTEMPO) radical system in benzene. CIDEP generation was reasonably explained in terms of the radical-triplet pair mechanism of singlet molecular oxygen-OTEMPO pair with doublet precursor. Several excited molecule-OTEMPO systems have been investigated if this CIDEP generation contributes to their CIDEP spectra. Surprisingly strong CIDEP was produced even in the presence of trace amount of dissolved oxygen, which suggests the importance of complete degassing for CIDEP studies in general systems.

III-N Dynamics of Excited Electronic States of 4-Dimethylaminopyridine and Its Derivatives

It is well known that some aromatic molecules with electronic donor and acceptor substituent groups such as 4-(dimethylamino)benzonitrile (DMABN) show peculiar dual fluorescence. The TICT (twisted intramolecular charge transfer) model is now widely accepted as the most plausible mechanism for the appearance of dual fluorescence. Besides the TICT model, however, various mechanisms have been proposed. For example, charge transfer from solute to solvent or change in the hybridization of orbitals of amino-nitrogen atom is discussed. Dynamics of the appearance of dual fluorescence, therefore, has not been clearly elucidated. DMABN and its derivatives have been only the systems so far whose dynamics of electronically excited states have been investigated in detail in relation to the TICT state formation. In this project, dynamics of 4-dimethylaminopyridine and its derivatives is investigated in detail in order to get more information on the appearance of dual fluorescence.

III-N-1 Dual Fluorescence of 4-Dimethylamino-pyridine and Its Derivatives in Solutions

Suguru MISHINA *(Tokyo Univ. Agric. Tech.)*, **Satoshi KUDOH** *(Tokyo Univ. Agric. Tech.)*, **Masao TAKAYANAGI** *(Tokyo Univ. Agric. Tech. and IMS)*, **Munetaka NAKATA** *(Tokyo Univ. Agric. Tech.)*, **Joe OTSUKI** *(Univ. Tokyo)* **and Koji ARAKI** *(Univ. Tokyo)*

Electronic absorption and emission spectra of 4-dimethylaminopyridine (DMAP), 3-methyl-4-dimethyl-aminopyridine (MDMAP), and 3,5-dimethyl-4-dimethylaminopyridine (DMDMAP) were measured in cyclohexane (non-polar), chloroform (medium polar), and acetnitrile (highly polar) solutions. These molecules are expected to show dual fluorescence. In MDMAP and DMDMAP, dimethylamino group and pyridine ring are expected to stay in a twisted position each other even in the ground electronic state because of the steric hindrance between the dimethylamino group and the methyl groups at 3 and 5 positions. Therefore, relation between dual fluorescence and twisting motion of the dimethylamino group can be investigated by comparing the spectroscopic behaviors of these three compounds. DMAP was of commercial origin, while MDMAP and DMDMAP were synthesized, respectively, from 4-nitro-3-picoline 1-oxide and 3,5-lutidine. Charge transfer (CT) emission at longer wavelength was observed for DMAP only in acetnitrile, while those for MDMAP and DMDMAP were observed in all the three solvents as shown in Figure 1. This result suggests that the TICT mechanism is valid; i.e. twisting motion of dimethylamino group plays the important role on the CT emission. Relative energies of LE (local excited) and CT states, which are considered to depend on the twisting angle between dimethylamino group and pyridine ring and on the solvent polarity, are discussed in detail.

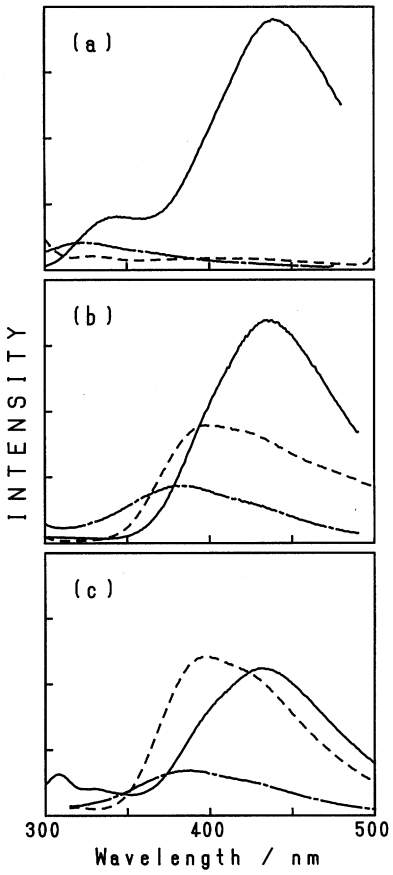

Figure 1. Emission spectra of (a) DMAP, (b) MDMAP, and (c) DMDMAP in acetnitrile (——), chloroform (– – –) and cyclohexane (–·–·–) solutions. Excitation wavelength was set at the absorption maximum around 280 nm for each solution.

III-O Conformation, Photoisomerization and Solvent Effect of Merocyanine Dyes

There has been increasing interest in the use of merocyanine dyes for photoelectric and photochemical devices. Although there have been a great deal of reports on the application of merocyanine dyes for devices, many questions still remain unanswered. For example, little has been known about the rotational isomerism of possible conformers in relation to the conjugated system. Although some merocyanine dyes show large solvent effect in their electronic absorption spectra, the effect has not been clearly interpreted in terms of intermolecular interaction and the structural change of dye molecules induced by solvents. In this project, resonance Raman, infrared absorption, electronic absorption, and fluorescence spectra of merocyanine dyes are measured in various solvents and in low-temperature Ar matrices to clarify their conformation and the mechanism of photoisomerization and solvent effect.

III-O-1 Dispersed Fluorescence and Fluorescence Excitation Spectra of Merocyanine Dyes in Low-Temperature Argon Matrices

Sumi KAWABATA *(Tokyo Univ. Agric. Tech.)*, **Masao TAKAYANAGI** *(Tokyo Univ. Agric. Tech. and IMS)*, **Munetaka NAKATA** *(Tokyo Univ. Agric. Tech.)*, **Yukihiro OZAKI** *(Kwansei-Gakuin Univ.)* **and Keiji IRIYAMA** *(The Jikei Univ. School of Medicine)*

Dispersed Fluorescence and fluorescence excitation spectra of the merocyanine dyes, 5-[2-(3-ethyl-2-benzothiazolylidene)-1-methyl-ethylidene]-3-ethyl-2-thioxo-4-thiazolidinone [Et(Me)MD] and 5-[2-(3-ethyl-2-benzothiazolylidene)ethylidene]-3-ethyl-2-thioxo-4-thiazolidinone [EtMD], in low-temperature argon matrices were measured. Four isomers in relation to the conjugated system are possible for each dye. They coexist in a solution where one isomer can be easily photoisomerized to another.[1)] It is difficult, therefore, to measure electronic absorption or fluorescence spectra of a single isomer of the dye molecules in solutions. Complexity due to the coexistence of isomers and photoisomerization can be avoided by applying the low-temperature matrix isolation technique because the photoisomerization is restricted in the matrices where a dye molecule is surrounded by inert solid rare gas. Fluorescence spectrum of a single isomer can be measured by choosing excitation wavelength, while electronic absorption spectrum of a single isomer can be measured as a fluorescence excitation spectrum by choosing the wavelength of observation.

Dye was vaporized by heating up to 120°C, mixed with argon, and deposited onto a CsI plate cooled at 15 K by a closed cycle helium refrigerator. Spectra of the

matrix sample were measured by a commercial fluorescence spectrophotometer (Shimadzu, RF-5300PC). Figure 1 shows the results for EtMD. These spectra are expected to give valuable information on the electronic structure and photoisomerization mechanism of the dyes.

Reference

1)M. Takayanagi, M. Nakata, Y. Ozaki, K. Iriyama and M. Tasumi, *J. Mol. Struct.* **405**, 239 (1997).

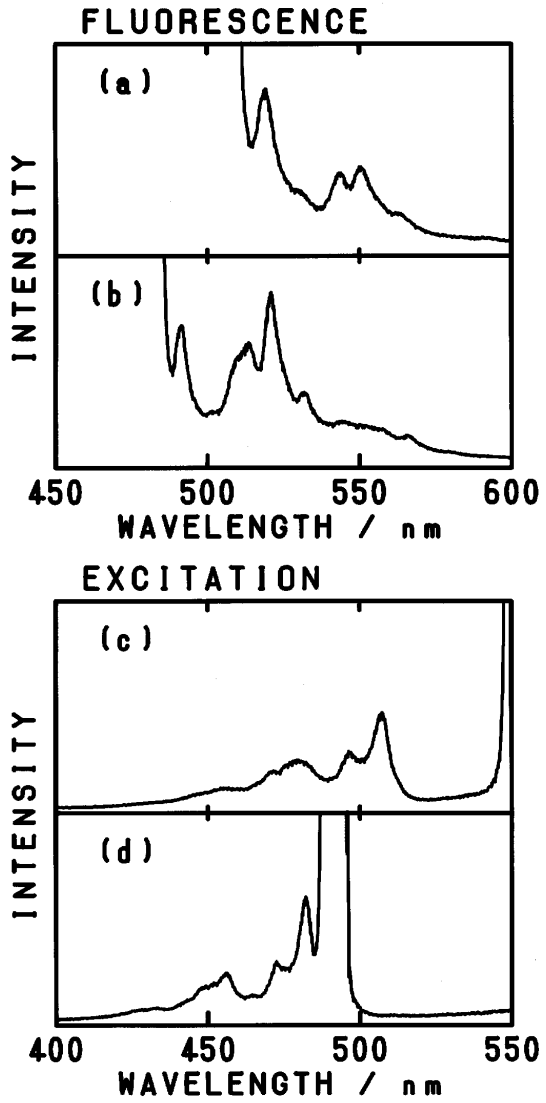

Figure 1. Spectra of EtMD in an Ar matrix. (a) and (b); dispersed fluorescence spectra measured by the excitation wavelengths of 507 and 482 nm, respectively. (c) and (d); fluorescence excitation spectra measured by probing 550 and 490 nm, respectively. Asterisks in (c) and (d) show the bands due to scattered light. Bands due to two isomers are overlapping in each spectrum.